Color-flavor dependence of the Nambu-Jona-Lasinio model and QCD phase diagram

Aftab Ahmad[†] Ali Murad[‡]

Institute of Physics, Gomal University, 29220, D.I. Khan, Khyber Pakhtunkhaw, Pakistan

Abstract: We study the dynamical chiral symmetry breaking/restoration for various numbers of light quarks flavors N_f and colors N_c using the Nambu-Jona-Lasinio (NJL) model of quarks in the Schwinger-Dyson equation framework, dressed with a color-flavor dependence of effective coupling. For fixed $N_f = 2$ and varying N_c, we observe that the dynamical chiral symmetry is broken when N_c exceeds its critical value $N_c^c \approx 2.2$. For a fixed $N_c = 3$ and varying N_f, we observe that the dynamical chiral symmetry is restored when N_f reaches its critical value $N_f^c \approx 8$. Strong interplay is observed between N_c and N_f, i.e., larger values of N_c tend to strengthen the dynamical generated quark mass and quark-antiquark condensate, while higher values of N_f suppress both parameters. We further sketch the quantum chromodynamics (QCD) phase diagram at a finite temperature T and quark chemical potential μ for various N_c and N_f. At finite T and μ, we observe that the critical number of colors N_c^c is enhanced, whereas the critical number of flavors N_f^c is suppressed as T and μ increase. Consequently, the critical temperature T_c, μ_c, and co-ordinates of the critical endpoint (T_c^E, μ_c^E) in the QCD phase diagram are enhanced as N_c increases and suppressed when N_f increases. Our findings agree with the lattice QCD and Schwinger-Dyson equations predictions.

Keywords: chiral symmetry breaking, Schwinger-Dyson equation, finite temperature and density, QCD phase diagram

DOI: 10.1088/1674-1137/ac6cd8

I. INTRODUCTION

Quantum chromodynamics (QCD) is a well-established theory of strong color interaction among quarks and gluons. Two major aspects of QCD are the asymptotic freedom (ultraviolet regime) [1, 2] and quark confinement (infrared regime) [3]. In asymptotic freedom, the quarks interact weakly at a short distance inside the hadrons. In contrast, at a large distance (or at low energy), the quarks are confined and never exist in isolation. In addition to color confinement, dynamical chiral symmetry breaking is another important property of low-energy QCD, which is related to the dynamical mass generation of quarks. It is well known that the QCD exhibits confinement and chiral symmetry breaking with a small number of light quark flavors N_f. However, for larger N_f, it is believed that a critical value N_f^c exists, above which the chiral symmetry restores and quarks become unconfined [4–6]. This N_f^c value must be smaller than the upper limit of the critical value where asymptotic freedom appears to exist, i.e., $N_f^{A,c} = (11/2)N_c$ [2]; for $N_c = 3$ with a gauge group $SU(3)$, this critical number is $N_f^{A,c} = 16.5$. Hence, the QCD theory is considered to be conformal in the infrared, guided by an infrared fixed point (i.e., a point at which the β-functions for the QCD couplings vanish); see for example for details [7–12]. The region $N_f^c \lesssim N_f < N_f^{A,c}$ is often called the "conformal zone" [4, 13]. At or near the upper end ($N_f \lesssim N_f^{A,c}$) of the conformal zone, the infrared fixed point lies in the weakly interacting region and can be solved using perturbative techniques of QCD. In contrast, around the lower end ($N_f \sim N_f^c$), the infrared fixed point shifts toward the strongly interacting region where the coupling is sufficiently strong as N_f decreases; thus, the system enters a phase in which the chiral symmetry breaks and quarks become confined. In this scenario, the perturbative approaches to QCD are inconceivable; thus, the nonperturbative techniques are useful tools. Lattice QCD simulations [5, 14–17], as well as the continuum meth-

Received 26 January 2022; Accepted 5 May 2022; Published online 20 June 2022

[†] E-mail: aftabahmad@gu.edu.pk

[‡] E-mail: alimuradeng@gmail.com

ods of QCD [6, 18–22], in the fundamental $SU(3)$ representation emphasize that the chiral symmetry restoration and deconfinement phases occur when N_f reaches the conformal zone $8 \lesssim N_f^c < 12$. QCD theory with a larger number of colors N_c in the fundamental $SU(N_c)$ representation also has a significant role in the infrared domain. Ref. [22] discussed that the chiral symmetry is dynamically broken above a critical value $N_c^c \approx 2.2$. The increasing N_c enhances the dynamical mass generation near and above N_c^c. A large N_c also effects the critical value of flavors N_f^c, that is, N_f^c shifts toward its higher values as N_c increases.

In addition to N_c and N_f, the infrared domain of QCD is also affected by the presence of heat baths. It is believed that at zero or low temperature T, the fundamental degrees of freedom of low-energy QCD are the color-singlet (confined) hadrons, whereas at high T, when T reaches its critical value T_c, the interaction becomes weaker, thus causing hadrons to melt into a new phase, where the quarks and gluons become the new degrees of freedom. The chiral symmetry is restored and deconfinement of quarks occurs in this new phase. Lattice QCD calculations [23– 29], the Schwinger-Dyson equation [30–39], and other effective models of low-energy QCD [40–46] indicate that the nature of this transition is a crossover in the presence of a finite current quark mass m. Similarly, when the quark chemical potential μ increases, the same physical picture prevails but the nature of the phase transition changes from crossover to first-order at some point, which is known as the critical endpoint in the QCD phase diagram, often drawn in the $T-\mu$ plane. Experimentally, there is a strong motivation toward the study of phase transitions in the Heavy-Ion Collision at the Large Hadron Collider (LHC) at CERN, the Relativistic Heavy Ion Collider (RHIC) at Brookhaven National Laboratory (BNL), and the Compressed Baryonic Matter (CBM) experiment. The study of low-energy QCD for higher quark flavors N_f and N_c also has a significant role in physics beyond the standard model (BSM), and its extension to the QCD phase diagram at finite T and μ, where different phases of QCD exist, i.e., quark-gluon plasma, quarkyonic matter, neutron star environment, and the color-flavor-locked region of the QCD phase diagram.

Our aim and motivation of this work was to investigate the critical N_c and N_f for the chiral symmetry breaking and restoration at zero T and finite T and μ. Furthermore, we are interested to draw the QCD phase diagram in the $T-\mu$ plane for various N_c and N_f. We use the effective Nambu-Jona-Lasinio (NJL) model [47], dressed with the number of quark flavors N_f and in the fundamental $SU(N_c)$ representation in the Schwinger-Dyson equations framework. The NJL model has several features and is commonly used in the literature. Dynamical chiral symmetry breaking and its restoration are some of the main features of this model. However, it does not support the phenomenon of quark confinement.

The remainder of this article is organized as follows: In Sec. II, we introduce the general formalism of the NJL model at $T=0$ and at finite T and μ. In Sec. III, we discuss the numerical solution of the gap equation to study dynamical chiral symmetry breaking and its restoration for higher N_c and N_f values. In Sec. IV, we present the numerical solution of the gap equation for higher N_c and N_f and at finite T. In Sec. V, we depict the numerical solution of the gap equation at finite μ for various N_c and N_f. In Sec. VI, we sketch the phase diagram in the $T-\mu$ plane for various N_c and N_f. Finally, in Sec. VII, we provide the summary and conclusions of this work.

II. GENERAL FORMALISM OF THE NJL MODEL

We begin the QCD in an effective manner through the NJL Lagrangian density [47]:

$$\mathcal{L} = \bar{q}(\mathrm{i}\,\partial\!\!\!/ - m)q + \frac{G_0}{2}[(\bar{q}q)^2 + (\bar{q}\mathrm{i}\gamma_5\vec{\tau}q)^2], \tag{1}$$

where q and $\bar{q}$ represent quark and antiquark fields, respectively. Here, $\partial\!\!\!/ = \gamma_\mu\partial^\mu$, where γ^μ are the Dirac (4×4) gamma matrices, and $\partial^\mu = -\mathrm{i}p^\mu$ (p^μ represents the four-momenta). Here, m is the bare light quark mass matrix, which may be equal to zero at the chiral limit. The four-fermion interaction in the square brackets contains a scalar and pseudoscalar interaction piece. $\vec{\tau}$ represents the Pauli matrix acting in isospin space. G_0 is the dimensionful effective coupling constant that can be obtained by considering the Fierz transformation of the color-current –color-current interaction $(-(\bar{q}\gamma^\mu\lambda^\alpha q)^2)$ (see Appendix A.3 in [41] or the Appendix of this paper).

Such a Lagrangian density Eq. (1) describes dynamical chiral symmetry breaking, which, in the Hartree (mean field) approximation can be triggered through the following gap equation:

$$M = m - 2G_0\langle\bar{q}q\rangle \quad \text{or} \quad \frac{M-m}{2G_0} = \langle\bar{q}q\rangle, \tag{2}$$

where M is the effective or dynamically quark mass, and $\langle\bar{q}q\rangle$ is the quark-antiquark condensate:

$$\langle\bar{q}q\rangle = -\mathrm{i}\int\frac{\mathrm{d}^4k}{(2\pi)^4}\mathrm{Tr}[S(k)]\,, \tag{3}$$

where "Tr" means the trace over Lorentz, color, and flavor matrices, and $S(k) = (\not{k} - M + \mathrm{i}\epsilon)^{-1}$ is the dressed-quark propagator (in Minkowski space) with $\mathrm{i}\epsilon$ being the causality factor, introduced to exclude the singularity from the propagator.

Substituting Eq. (3) into Eq. (2) and after performing

the traces, we obtain

$$M = m + 8\mathrm{i}G_0 N_f N_c \int \frac{\mathrm{d}^4k}{(2\pi)^4}\frac{M}{k^2 - M^2 + \mathrm{i}\epsilon}. \tag{4}$$

The gap equation Eq. (4) is based on the NJL Lagrangian. Eq. (1) describes the dynamical mass generation for N_f and N_c [1)].

In this work, we are interested to include the anti-screening effects of the gluons and the screening effects of the light quarks; we extend the NJL model to an $SU(N_c)$ gauge theory with an N_f number of light quarks. In this connection, we can determine the critical number of flavors or colors for the dynamical chiral symmetry breaking/restoration using an "NJL-type" model in the Schwinger-Dyson equations (SDE) framework. In the SDE scenario, the dynamical mass can be obtained from the dressed quark propagator:

$$S^{-1}(p) \quad = S_0^{-1}(p) + \Sigma(p), \tag{5}$$

where $S_0(p) = (\not{p} - m + \mathrm{i}\epsilon)^{-1}$ is the bare quark propagator, and $S(p)$ is the dressed quark propagator. The self energy $\Sigma(p)$ is given by

$$\Sigma(p) = -\mathrm{i}\int \frac{\mathrm{d}^4k}{(2\pi)^4} g^2 D_{\mu\nu}(q)\frac{\lambda^a}{2}\gamma_\mu S(k)\frac{\lambda^a}{2}\Gamma_\nu(p,k), \tag{6}$$

where g^2 is the QCD coupling constant, and $\Gamma_\nu(k,p)$ is the dressed quark-gluon vertex. Here, $D_{\mu\nu}(q) = D(q)(-\mathrm{i}g_{\mu\nu} - \frac{q_\mu q_\nu}{q^2})$ is the gluon propagator in the Landau gauge, with $g_{\mu\nu}$ being the metric tensor in the Minkowski space; $q = k - p$ is the gluon four momentum, and $D(q)$ is the gluon scalar function. λ^a, s are the usual Gell-Mann's matrices. In the $SU(N_c)$ representation, the Gell-Mann's matrices satisfies the following identity:

$$\sum_{a=1}^{8}\frac{\lambda^a}{2}\frac{\lambda^a}{2} = \frac{1}{2}\left(N_c - \frac{1}{N_c}\right)I, \tag{7}$$

where I is the unit matrix. We use the following form of the gluon propagator (in Landau gauge), in the infrared region where the gluons dynamically acquire a mass Λ_g^2 ($\sim 500 \pm 200$ MeV) [48, 49] and bare vertex approximation ($\Gamma_\nu(k,p) = \gamma^\nu$) (see for example [22, 50, 51]):

$$g^2 D(q \to 0) = \frac{4\pi\alpha_{ir}}{\Lambda_g^2} = G, \tag{8}$$

which ensures the mapping of one-gluon exchange diagrams to a contact interaction in the NJL model. With a particular choice of the gap equation kernel, the dynamical quark mass function is merely a constant, and the dressed quark propagator takes the form [52]

$$S(k) = \frac{\not{k} + M}{k^2 - M^2 + \mathrm{i}\epsilon}. \tag{9}$$

The effective coupling G must exceed its critical value G_c to describe dynamical chiral symmetry breaking. When G is greater than G_c, a nontrivial solution to the QCD gap equation bifurcates from the trivial one (see for example [53]). In this work, we use the effective coupling $G = 7.05 \times 10^{-6}\mathrm{MeV}^{-2}$ [2)], which can be obtained by setting the gluon mass scale $\Lambda_g = 587.9$ MeV [41] and $4\pi\alpha_{ir} = 2.44$. Substituting Eqs. (6)–(9) into Eq. (5) and taking the trace over the Dirac, colors, and flavors components, the gap equation is given by

$$M = m + 8\mathrm{i}\mathcal{G}^{N_c}(N_f)\int \frac{\mathrm{d}^4k}{(2\pi)^4}\frac{M}{k^2 - M^2 + \mathrm{i}\epsilon}. \tag{10}$$

Thus, our truncation of the Schwinger-Dyson equations is equivalent to that of the NJL model in the Hartree mean field approximation, where $\mathcal{G}^{N_c}(N_f)$ is the effective coupling in which the color and flavor factors are incorporated as

$$\mathcal{G}^{N_c}(N_f) = \left[\frac{1}{2}\left(N_c - \frac{1}{N_c}\right)\right]G(N_f). \tag{11}$$

To study the gap equation for the various number of flavors, we must modify the flavor sector $G(N_f)$ of the effective coupling $\mathcal{G}^{N_c}(N_f)$ in a manner that it provides us the solution to the gap equation for the higher number of flavors. We shall use this modification as our modeling and it will aid us in determining N_f^c or N_c^c for chiral symmetry breaking or restoration. We adopt a similar method of modeling used by [5, 22] in which N_f^c are obtained from Schwinger-Dyson equations. According to [5, 22], the dynamically generated mass M should have the following type of relationship with N_f^c:

$$M \backsim \sqrt{1 - \frac{N_f}{N_f^c}}, \tag{12}$$

where N_f^c is the critical number of flavors. To obtain such

1) The way the gap equation Eq. (4) is written (or obtained) may be or may not sufficient to describes the dynamical symmetry breaking for $N_f = 0$ or $N_c = 0$ (or smaller to larger values of N_f and N_c). This is one of the reason that we used SDE treatment of the NJL model where we can modified the effective coupling in such a way that our gap equation describes the dynamical chiral symmetry breaking/restoration for $N_f = 0$ to larger N_f and from smaller N_c to its larger values.

2) We use the different symbols for the effective coupling G (which is the ratio of the QCD coupling to the gluon mass scale) that appeared in the SDE, and dressed it with flavors and colors number to distinguish it from G_0 that appeared in the NJL gap equation.

a behavior in the four-fermion contact interaction NJL model, only a square root flavor-dependence in the coupling results in this observed behavior [22]. Therefore, to determine N_f^c, we modify the factor $G(N_f)$ of Eq. (11) in similar fashion as in [22]:

$$G(N_f) \longrightarrow \frac{9}{2}G\sqrt{1-\frac{(N_f-2)}{\mathcal{N}_f^c}}, \tag{13}$$

where $\mathcal{N}_f^c = N_f^c + \eta$ is a guess value of the critical number of flavors. Our modification of the effective coupling is almost the same as in [22] but slightly different by a factor of 9/2 This is because the effective coupling model of [22] uses a local symmetry preserving four-point contact interaction, which, in the scalar-pseudoscalar channel, is Fierz equivalent to the term in NJL-Lagrangian Eq. (1) [42], (for Fierz transformation, see for example Appendix A in [41] and the Appendix at the end of this article).

To obtain N_f^c, we set $\eta = 2.3$ which lies in the range as predicted in [22] by considering $N_f^c = 8$. Ref. [22] demonstrated that the parameter η appears because of the factor $(N_f - 2)$ in Eq. (13). For fixed $N_c = 3$ and $N_f = 2$, our modified NJL effective coupling $\mathcal{G}^{N_c}(N_f) \to GN_fN_c$ that normally used in NJL model gap equation Eq. (4).

The four-momentum integral in Eq. (10) can be solved by splitting the four-momentum into time and space components. We denote the space part by a bold face letter $\mathbf{k}$ and the time part by k_0. Thus, Eq. (10) can be expressed as

$$\begin{aligned} M =& m + 8\mathrm{i}\mathcal{G}^{N_c}(N_f)M\int_0^{\infty}\frac{\mathrm{d}^3\mathbf{k}}{(2\pi)^4} \\ &\times\int_{-\infty}^{+\infty}\frac{\mathrm{d}k_0}{{k_0}^2 - E_k^2 + \mathrm{i}\epsilon}. \end{aligned} \tag{14}$$

Here, $E_k = \sqrt{|\mathbf{k}|^2 + M^2}$, in which E_k denotes the energy per particle, and $\mathbf{k}$ is the 3-momentum. On integrating over the time component of Eq. (14), we obtain the following expression:

$$M = m + 8\mathrm{i}\mathcal{G}^{N_c}(N_f)M\int_0^{\infty}\frac{\mathrm{d}^3\mathbf{k}}{(2\pi)^4}\frac{\pi}{\mathrm{i}E_k} \tag{15}$$

In spherical polar coordinates, $\mathrm{d}^3\mathbf{k} = \mathbf{k}^2\mathrm{d}\mathbf{k}\sin\theta\mathrm{d}\theta\mathrm{d}\phi$, and performing the angular integration, we obtain from Eq. (15)

$$M = m + \frac{2\mathcal{G}^{N_c}(N_f)M}{\pi^2}\int_0^{\infty}\mathrm{d}\mathbf{k}\frac{\mathbf{k}^2}{E_k}. \tag{16}$$

The integral occurring in Eq. (13) is a diverging integral, and we also know that the NJL model is not renormalizable owing to fermionic contact interaction. Different types of regularization schemes are used in the literature [40]. The regularization procedure we adopt in the present scenario is the three-dimensional (3d) momentum cut-off in which we remove the divergence by applying a certain high ultraviolet 3d-momentum cut-off Λ. Thus, Eq. (16) can be expressed as

$$M = m + \frac{2\mathcal{G}^{N_c}(N_f)M}{\pi^2}\int_0^{\Lambda}\mathrm{d}\mathbf{k}\frac{\mathbf{k}^2}{E_k}. \tag{17}$$

After integrating over the time component in Eq. (17), we obtain

$$M = m + \frac{\mathcal{G}^{N_c}(N_f)M}{\pi^2}\left[\Lambda\sqrt{\Lambda^2+M^2} - M^2\mathrm{arcsinh}\left(\frac{\Lambda}{M}\right)\right]. \tag{18}$$

In the present scenario, the quark-antiquark condensate, which serves as an order parameter for the chiral symmetry breaking, is defined as

$$-\langle\bar{q}q\rangle = \frac{M-m}{2\mathcal{G}^{N_c}(N_f)}. \tag{19}$$

The finite T and μ version of the NJL-model gap equation Eq. (10) can be obtained by adopting the standard convention for momentum integration i.e.,

$$\int\frac{\mathrm{d}^4k}{\mathrm{i}(2\pi)^4}f(k_0,\mathbf{k}) \to T\sum_n\int\frac{\mathrm{d}^3k}{(2\pi)^3}f(\mathrm{i}\omega_n+\mu,\mathbf{k}), \tag{20}$$

where $\omega_n = (2n+1)\pi T$ are the fermionic Matsubara frequencies. After performing some algebra, the gap equation Eq. (10) at finite T and μ can be expressed as

$$M = m + 4\mathcal{G}^{N_c}(N_f)M\int_0^{\Lambda}\frac{\mathrm{d}^3\mathbf{k}}{(2\pi)^3}\frac{1}{E_k}(1 - n_{\mathrm{F}}(T,\mu) - \bar{n}_{\mathrm{F}}(T,\mu)), \tag{21}$$

which is similar to Eq. (18) in a vacuum but modified by the thermo-chemical parts. $n_{\mathrm{F}}(T,\mu)$ and $\bar{n}_{\mathrm{F}}(T,\mu)$ represent the Fermi occupation numbers for the quark and antiquark, respectively, and are defined as

$$\begin{aligned} n_{\mathrm{F}}(T,\mu) &= \frac{1}{\mathrm{e}^{(E_k-\mu)/T}+1}, \\ \bar{n}_{\mathrm{F}}(T,\mu) &= \frac{1}{\mathrm{e}^{(E_k+\mu)/T}+1}. \end{aligned} \tag{22}$$

On further simplifying, we obtain

$$M = m + \frac{\mathcal{G}^{N_c}(N_f)M}{\pi^2}\left[\Lambda\sqrt{\Lambda^2+M^2} - M^2\,\mathrm{arcsinh}\left(\frac{\Lambda}{M}\right)\right] - \frac{\mathcal{G}^{N_c}(N_f)M}{\pi^2}\int_0^{\Lambda} \mathrm{d}\mathbf{k}\frac{\mathbf{k}^2}{E_k}\left[n_{\mathrm{F}}(T,\mu)+\bar{n}_{\mathrm{F}}(T,\mu)\right]. \quad (23)$$

If we set $\mu = T = 0$ in Eq. (23), we obtain$n_{\mathrm{F}} = \bar{n}_{\mathrm{F}} = 0$; thus, we can retain the gap equation in vacuum, i.e., Eq. (18). In the next section, we present a numerical solution of Eq. (18) for higher numbers of colors and flavors.

III. DYNAMICAL CHIRAL SYMMETRY BREAKING/RESTORATION FOR N_c AND N_f

In this section, we numerically solve the gap equation Eq. (18) with a particular choice of the parameters, i.e., the cutoff parameter $\Lambda = 587.9$ MeV[1)], $G = 7.05\times 10^{-6}$ MeV^{-2}, and $m = 5.6$ MeV, which have been determined to reproduce the pion decay constant $f_\pi = 92.4$ MeV and pion mass $m_\pi = 135.0$ MeV in the two-flavors NJL model [41]. The solution of our gap equation with modified color-flavor dependence effective coupling Eq. (11) for two light flavors $N_f = 2$ (i.e., up and down) and for $Nc = 3$ yields the dynamical mass $M = 399$ MeV. From Eq. (19), we calculate the corresponding quark-antiquark condensate as $-\langle\bar{q}q\rangle^{1/3} = 250$ MeV. In this scenario, our results are consistent with that obtained in [41]. Next, we solve the gap equation Eq. (18), for various N_c and N_f. Initially, we solve the gap equation for fixed $N_f = 2$ but varying N_c and plot the dynamically generated quark mass in Fig. 1(a) as a function of N_c. We observe that the chiral symmetry is dynamically broken when N_c exceeds a critical value, $N_c = N_c^c$, and remains broken for larger values of N_c. The corresponding quark-antiquark condensate $-\langle\bar{q}q\rangle^{1/3}$ is shown in Fig. 1(b). N_c^c is obtained from the peak of the color gradient of the quark-antiquark condensate $-\partial_{N_c}\langle\bar{q}q\rangle^{1/3}$ and is depicted in Fig. 1(c), from which we observe that the chiral symmetry is dynamically broken above $N_c^c \approx 2.2$nd is thus consistent with the predicted value obtained in [22]. Next, we fix $N_c = 3$ and solve Eq. (18) for various N_f as shown in Fig. 2(a). The plot demonstrates that the dynamically generated mass monotonically decreases with the increase in N_f until it reaches a critical value N_f^c, where the dynamical mass vanishes and only bare quark mass survives; thus, chiral symmetry is dynamically restored

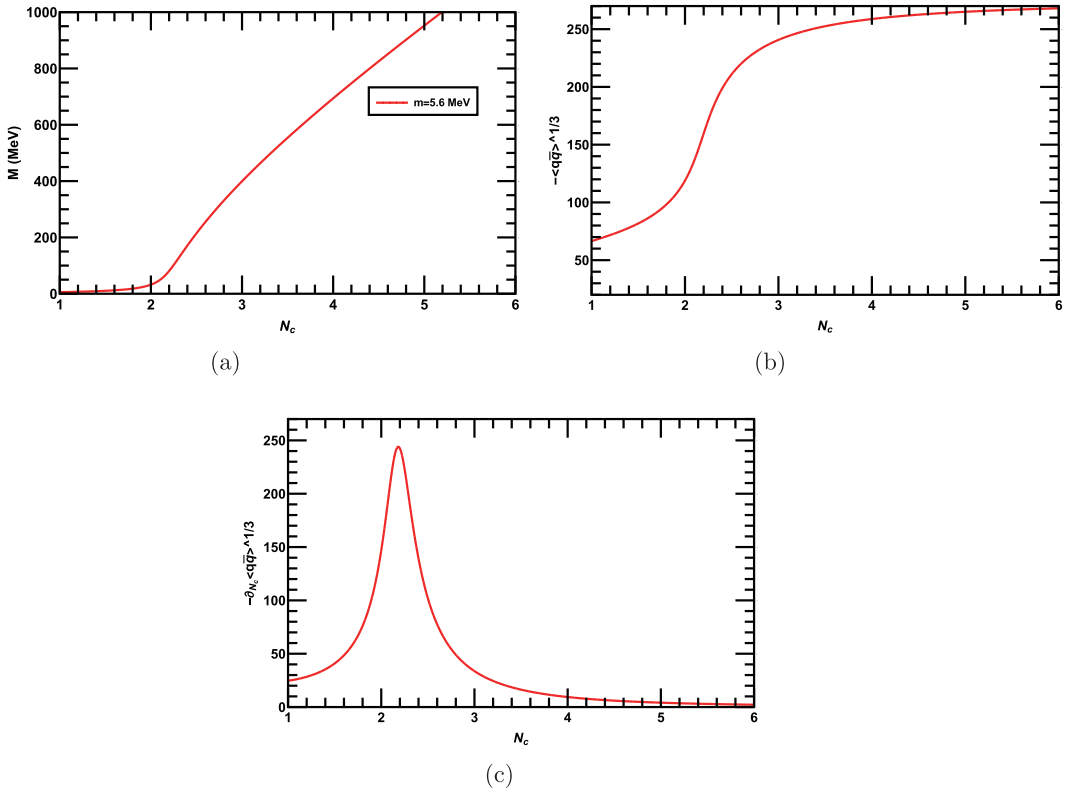

Fig. 1. (color online) (a) Behaviors of dynamical qurak mass as a function of number of colors N_c for two fixed flavors $N_f = 2$. (b) Quark-antiquark condensate as a function of N_c. (c) Color gradient of the quark-antiquark condensate; the peak of the gradient is at $N_c \approx 2.2$, which is the critical number for dynamical chiral symmetry breaking.

1) It should be noted that we have used the same numerical value of cut-off parameter and the gluon mass scale $\Lambda = \Lambda_g = 587.9$ MeV.

when N_f exceeds N_f^c. In Fig. 2(b), we plot $-\langle\bar{q}q\rangle^{1/3}$ as a function of N_f, and its flavor gradient $-\partial_{N_f}\langle\bar{q}q\rangle^{1/3}$ is depicted in Fig. 2(c). Thus, we obtain $N_f^c \approx 8$ from the peak of the flavor gradient $-\partial_{N_f}\langle\bar{q}q\rangle^{1/3}$. Our results in this scenario agree with that obtained in [22]. In Fig. 3, we plot the critical line between N_f and N_c in the $N_c - N_f$ plane; both the parameters opposes the effect of each other. Fig. 3 clearly demonstrates that the N_f^c required for dynamical chiral symmetry restoration increases as N_c increases, and as N_f increases, the N_c^c required for the dynamical chiral symmetry breaking increases. For better understanding, we have tabulated some data for the variation in N_f^c with various N_c^c in Table 1. In the next section, we discuss the dynamical chiral symmetry breaking and its restoration with N_c and N_f at finite T.

IV. DYNAMICAL CHIRAL SYMMETRY BREAKING WITH N_c AND N_f AT FINITE T

In this section, we numerically solve the gap equation Eq. (23) to understand dynamical symmetry breaking and restoration for various Nc and N_f and at finite T. Initially, we fix $N_f = 2$ and plot the dynamical mass in Fig. 4(a) as a function of N_c for various T. The corresponding condensate is depicted in Fig. 4(b). We observe that as T increases, the dynamical symmetry is broken above N_c^c. We determine the N_c^c for various values of T from the peaks of the color gradient $-\partial_{N_c}\langle\bar{q}q\rangle^{1/3}$, as shown in Fig. 4(c). The peaks of the gradient shift towards larger values of N_c as we increase T. Hence, N_c tends to enhance the dynamical quark mass and condensate while T suppresses both, and as a result, we require higher values of N_c for dynamical chiral symmetry breaking. Thus, N_c^c increases with T, as shown in the phase diagram drawn in the $N_c - T$ plane in Fig. 4(d). This means that in the presence of a heat bath, a large N_c^c is required for dynamical chiral symmetry breaking. The nature of the transition at each temperature $T = T_c$ is of crossover.

Now, for fixed $N_c = 3$, we plot the dynamical mass as a function of N_f for different values of T as shown in Fig. 5(a), and the corresponding condensate is depicted in Fig. 5(b). In this case, we observe that the dynamical mass as a function of N_f is suppressed as T increases. We obtain the critical number of flavors N_f^c for different T from the peaks of the flavor gradient $-\partial_{N_f}\langle\bar{q}q\rangle^{1/3}$, as shown in Fig. 5(c). We observe that the peaks shifted towards their smaller N_f values. Thus, N_f^c monotonically decreases as T increases, as demonstrated in the phase

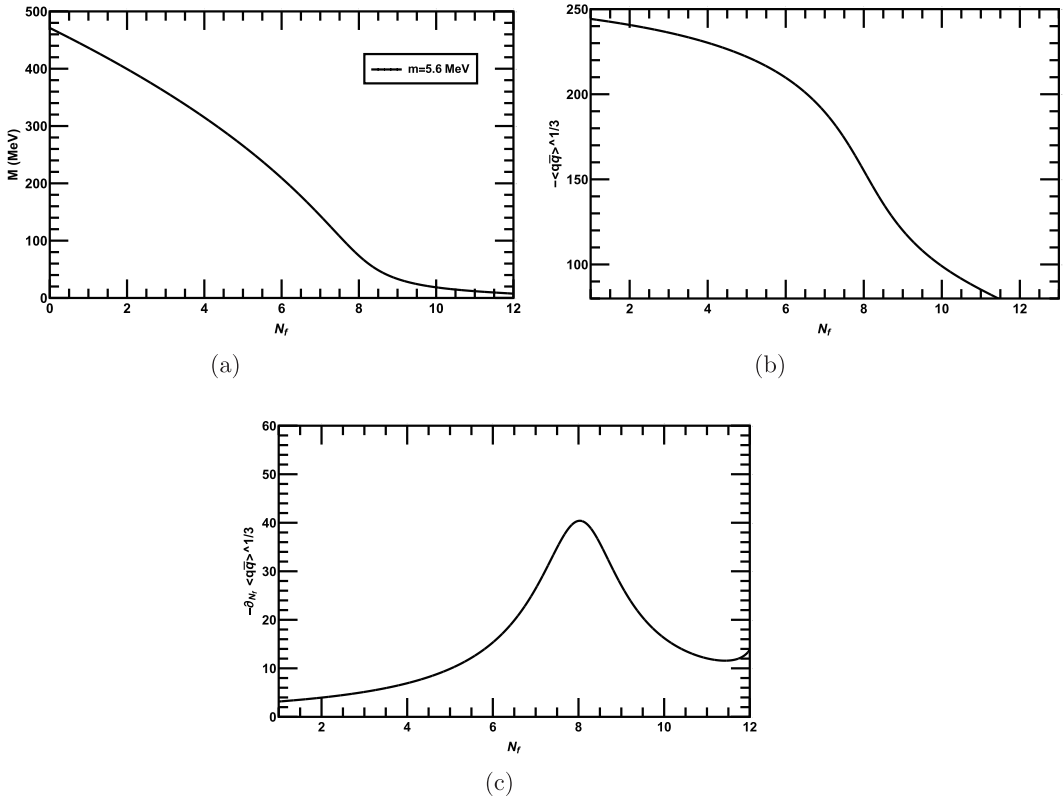

Fig. 2. (a) Behavior of the dynamical mass as a function of various N_f for fixed $N_c = 3$. The dynamical mass monotonically decreases with increasing N_f. (b) Quark-antiquark condensate as a function of N_f. (c) Flavor gradient of the quark-antiquark condensate as a function of N_f. The peak of the gradient is at $N_f \approx 8$, which is the critical number of flavors N_f^c, above which the dynamical chiral symmetry is restored.

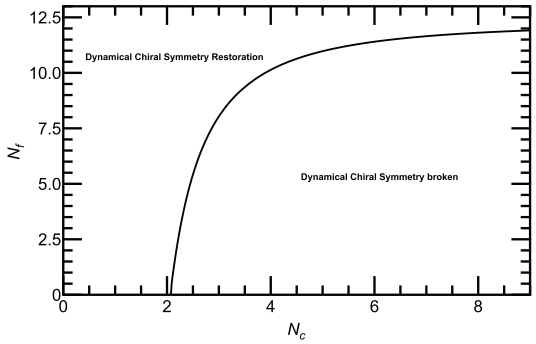

Fig. 3. Plot of the critical line between N_f and N_c in the $N_c - N_f$ plane.

Table 1. Data for plotting the critical line in the $N_c - N_f$ plane as depicted in Fig. 3.

N_c	2.2	3	4	5	6	7	8	9	10
N_f	3	8	9.5	10.3	10.7	11	11.2	11.3	11.4

diagram in the $N_f - T$ plane in Fig. 5(d). Therefore, in the presence of a heat bath, a lower N_f^c is required for dynamical chiral symmetry breaking/restoration. The nature of the transition at each temperature T is of crossover. In the next section, we investigate the behavior of chiral symmetry breaking and restoration at a finite chemical potential μ, for various N_c and N_f.

V. DYNAMICAL CHIRAL SYMMETRY BREAKING FOR N_f, N_c, AND AT FINITE μ

In this section, we discuss dynamical chiral symmetry breaking and its restoration at a finite μ for various N_c and N_f. The dynamical mass as a function of μ for fixed $N_f = 2$ and various N_c is shown in Fig. 6(a). We observe that the chiral symmetry is dynamically restored when μ exceeds a critical value μ_c. The discontinuity in the dynamical mass at $\mu = \mu_c$ shows that the nature of the phase transition is of first-order, while the smooth decrease in the dynamical mass represents the crossover transition. This means that μ suppresses the dynamical mass and condensate in contrast to N_c, which strengthens it. We can determine the critical number of colors N_c^c from the peak of $-\partial_{N_c}\langle\bar{q}q\rangle_\mu^{1/3}$ for various μ. We plot the phase diagram in the $N_c - \mu$ plane, where we show the variation in N_c^c with μ in Fig. 6(b). This plot shows that as we increase μ, N_c^c also increases. For example, at $\mu = 100$ MeV, we require a lower critical number of colors (i.e,

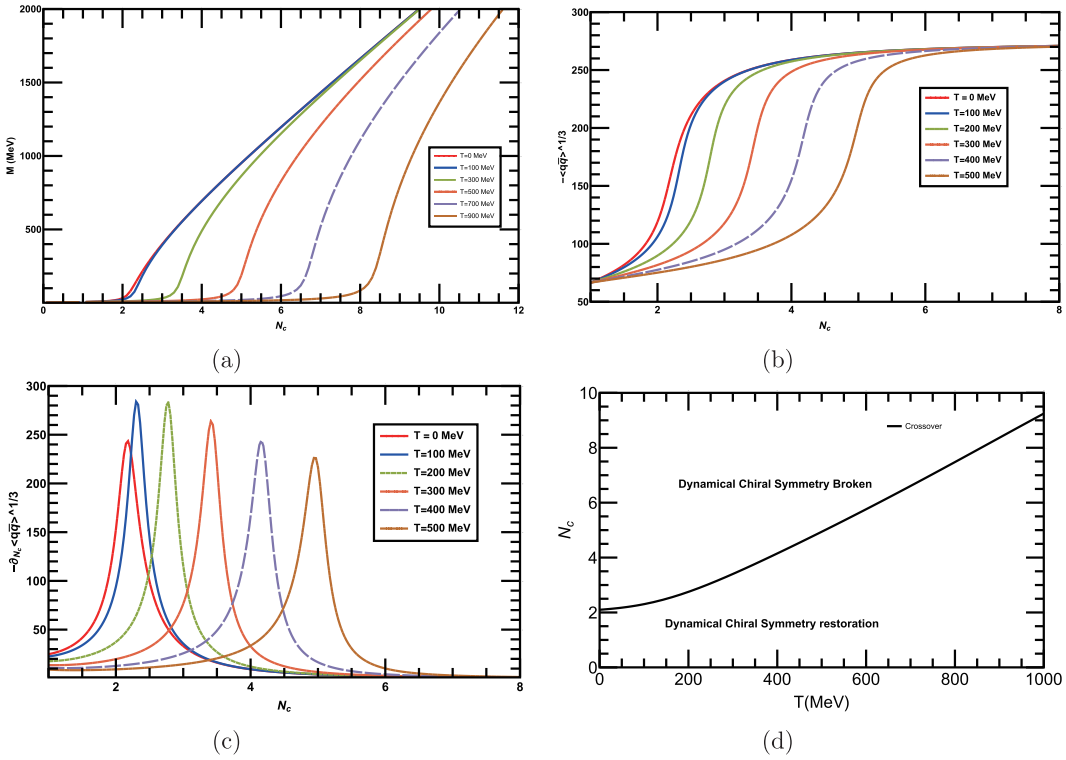

Fig. 4. (color online) (a) Behavior of dynamical mass as a function of N_c for fixed $N_f = 2$ and for various T. (a) Quark-antiquark condensate as a function of N_c for various T and fixed $N_f = 2$. (c) Color gradient of quark-antiquark condensate for various T. The peaks of the gradient shifts towards their larger values of N_c as T increases. (d) Phase diagram for dynamical chiral symmetry breaking/restoration in the $N_c - T$ plane. The higher the T, the larger value of N_c required for the dynamical symmetry breaking.

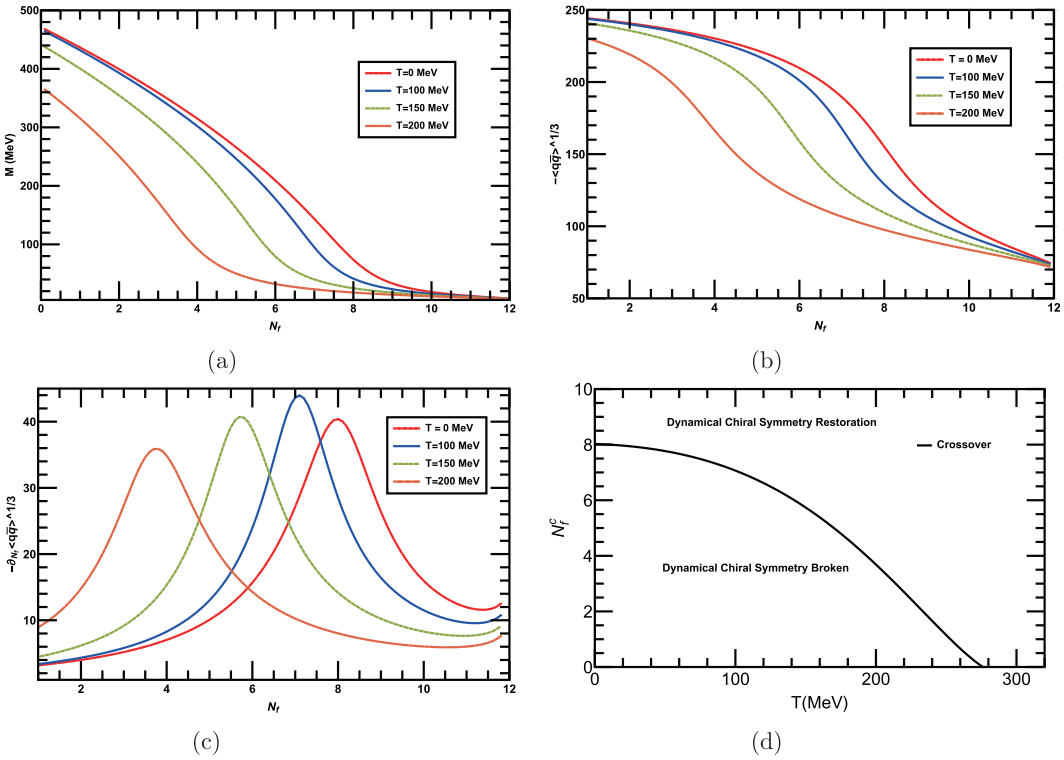

Fig. 5. (color online) (a) Behavior of dynamical mass as a function of N_f for fixed $N_c = 3$ and various T. As T increases, the dynamical mass is suppressed. (b) Behavior of the quark-antiquark condensate as a function of N_f for various T. (c) Flavor gradient of the condensate for various T, which shows that as T increases, the peaks shift towards their lower N_f values. (d) Phase diagram for the dynamical chiral symmetry breaking/restoration in the $N_f - T$ plane.

$N_c^c = 2.2$) for chiral symmetry breaking compared with $\mu = 250$ MeV (i.e., $N_c^c = 2.5$). We observe the crossover phase transition for $N_c \leq 2.5$ and first-order transition for $N_c > 2.5$ differentiated by a critical endpoint ($N_c^c \approx 2.5$, $\mu_c^c \approx 290$ MeV). Next, we fix $N_c = 3$ and plot the dynamical mass as a function of μ for various N_f in Fig. 7(a). Dynamical chiral symmetry is restored when the chemical potential reaches a critical value μ_c for different N_f. However, the nature of phase transition is of first-order for $N_f \leq 5$ and crossover for $N_f \geq 5$. The dynamical mass as a function of μ is suppressed with the increase in N_f. We then determine the critical number of flavors N_f^c for each chemical potential μ from the peak of $-\partial_{N_c}\langle\bar{q}q\rangle_\mu^{1/3}$ and plot the variation in N_f^c versus μ_c in the $N_f - \mu$ plane, as depicted inFig. 7(a). We note that N_f^c decreases with the increase in μ. The nature of the phase transition is crossover until the critical endpoint ($N_c^f = 5, \mu_c^f = 290$ MeV) where at and above it, the nature of transition changes to first-order.

The overall results shows that at higher values of μ, we require a higher N_c^c and lower N_f^c for dynamical chiral symmetry breaking/restoration. In the next section, we investigate the simultaneous effects of T and μ on chiral phase transition for various N_c and N_f.

VI. QCD PHASE DIAGRAMS FOR VARIOUS N_c AND N_f IN THE T–μ PLANE

In this section, we sketch the QCD phase diagrams in the $T - \mu$ plane for various N_c and N_f. First, the QCD phase diagram is shown in Fig. 8 for fixed $N = 2$ and for various number of colors (i.e, $N_c = 3,4,5,6$) at T and μ. We obtain the critical temperature T_c and critical chemical potential μ_c from the peaks of the thermal and chemical potential gradients of the quark-antiquark condensate, receptively. Initially, we plot the phase diagram for $N_f = 2$ and $N_c = 3$, which shows that at finite T but at $\mu = 0$, the dynamical chiral symmetry is broken for $T \leq T_c \approx 235$ MeV, while above that, it is restored. The phase transition is a crossover in this case. At finite μ and $T = 0$, the dynamical symmetry is observed to be broken below $\mu_c \approx 380$ MeV, while above that, it is restored via first-order phase transition. We confirm from Fig. 8 that the crossover line in the phase diagram starts from a finite T-axis (for $\mu = 0$) never ends up at finite μ-axis (for $T = 0$); hence, a critical endpoint exists at which the crossover transition changes to first-order transition. We determine the co-ordinates of the critical endpoint at ($\mu_c^E \approx 330, T_c^E \approx 81$) MeV. Our analysis for $N_f = 2$ and $N_c = 3$, with a particular choice of parameters of NJL-type model, which is based on the SDE truncation, is con-

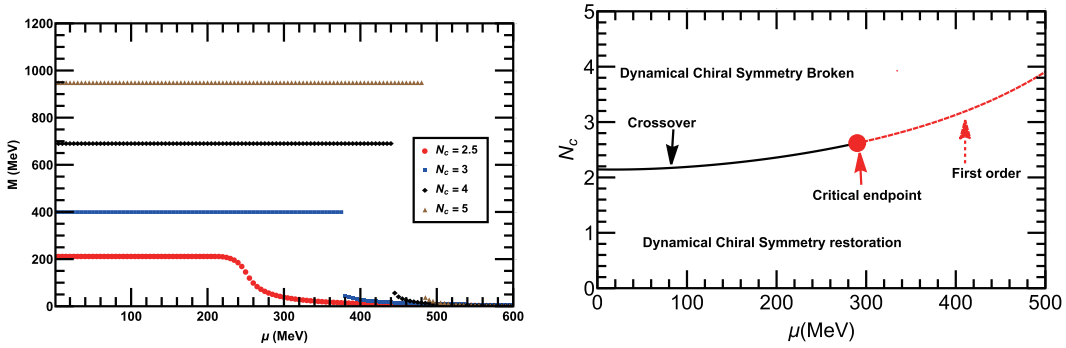

(a) (b)

Fig. 6. (color online) (a) Dynamical quark mass as a function of μ for various N_c and fixed $N_f = 2$. The plot shows that the dynamical mass decreases as we increase μ. The discontinuity in the mass function for $N_c \geq 2.5$ demonstrates that the nature of the phase transition is of first-order, while that of $N_c < 2.5$ is crossover. (b) Phase diagram for dynamical chiral symmetry breaking/restoration in the $N_c - \mu$ plane. The nature of the phase transition is of smooth crossover until the critical endpoint ($N_c^c \approx 2.5, \mu_c^c \approx 290$ MeV), while above it, the transition changes to the first-order.

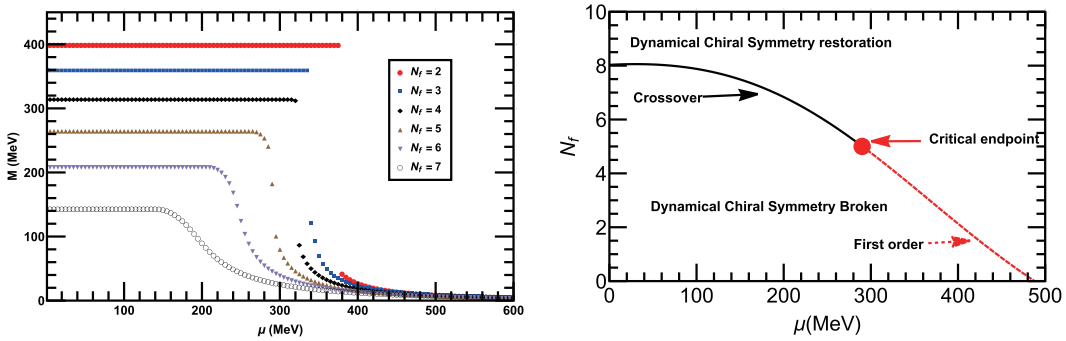

(a) (b)

Fig. 7. (color online) (a) Behavior of the dynamical quark mass as a function of μ at various N_f and fixed $N_c = 3$. The plot demonstrates that the dynamical chiral symmetry is restored above a critical μ_c for each N_c. (b) Phase diagram for dynamical chiral symmetry breaking/restoration in the $N_f - \mu$ plane. The nature of the phase transition is smooth crossover for $N_f < 5$ and changes to first-order for $N_f \geq 5$. Both transitions are differentiated by a critical endpoint ($N_c^f \approx 5$, $\mu_c^f \approx 290$ MeV).

sistent with that of the NJL model QCD phase diagram sketched in [41]. Subsequently, we extend it to various N_c. The solid-triangular lines represents the crossover phase transition for various N_c phase diagrams, and the dotted dashed lines for the first-order phase transition is separated by the big red dots (the critical endpoints) in all the phase diagrams. We observe that T_c, μ_c, and co-ordinates of the critical endpoints (μ_c^E, T_c^E) are shifted towards their higher values as N_c increases. The variation in T_c, μ_c, and (μ_c^E, T_c^E) with N_c are tabulated in Table 2. This means that as N_c increases, the strength of the non-abelian interaction increases. A higher N_c provides stronger bindings between the quarks. To undo that effect, we require a higher T or μ for the dynamical chiral symmetry breaking/restoration, as Fig. 8 confirms. Refs. [54, 55] demonstrated that μ_c increases with N_c as $\mu_c \sim \sqrt{N_c}$. Additionally, effective lattice simulations with heavy quarks have indicated the same observation about the shifting of critical endpoint in the phase diagram for higher N_c [56, 57]. Ref. [58] argued that T_c increases with N_c as $T_c \sim \sqrt{N_c}$. However, a lattice simulation of $SU(N_c)$ in the quenched approximation, based on the string tension σ, predicted an opposite behavior, i.e., $T_c(\mu = 0)/\sqrt{\sigma}$ decreases as N_c increases, and the transition is first-order at T_c [59], for more clear demonstration, see for example [60][1)], whereas, in the real-world for $N_c = 3$ and $N_f = 2$, the QCD exhibits a crossover transition near T_c [61].

Next, we draw the QCD phase diagrams in Fig. 9 for fixed $N_c = 3$ but various numbers of light quark flavors

1) In quenched lattice QCD, there are N_c^2 gluonic degrees of freedom but only N_c fermionic ones, as N_c becomes large the gluons dominate the dynamics and the fermions quenched out. So, in the large $N_c \to \infty$, QCD behaves like a pure gauge theory, and in this limit, the quenched QCD exhibits a first-order transition. As for as our NJL-type interaction concerned with dynamical quarks, based on the notion of single massive gluon exchanged between the quark-antiquarks with $g^2 N_c^2 \sim N_c$ and contributes to an Hartree potential. It could be if the link is actually realized by a single gluon exchange then the situation may changes.

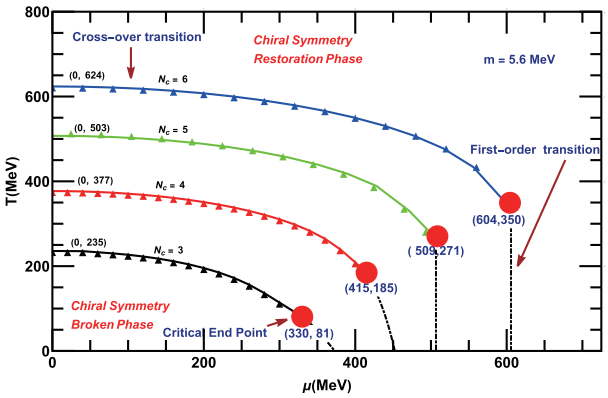

Fig. 8. (color online) QCD phase diagram in the $T-\mu$ plane for various number of colors ($N_c = 3,4,5,6$) and for fixed flavor $N_f = 2$. The all solid-triangle lines represent the crossover phase transitions, and the dot-dashed lines represent the first-order phase transitions. The big red-dots for the critical endpoints in each phase diagrams.

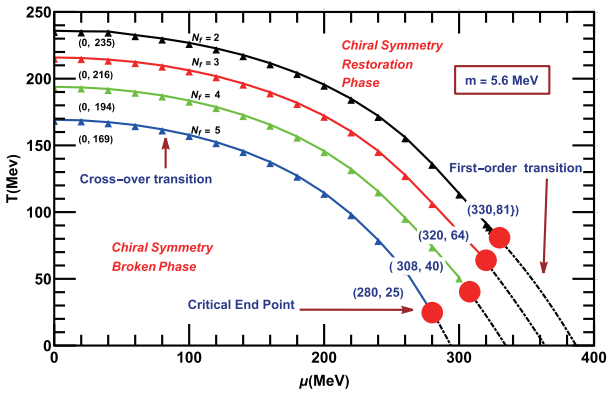

Fig. 9. (color online) QCD phase diagram for the $T_c-\mu_c$ plane for various number of flavors ($N_c = 2,3,4,5$), for fixed $N_c = 3$. All solid-triangle lines represent the crossover phase transitions and dot-dashed lines the first-order phase transition. The big red-dots represent the location of the critical endpoint in each phase diagram.

Table 2. Data for the variation in T_c and (μ_c^E, T_c^E) in the phase diagrams with various N_c, for fixed $N_f = 2$ and $m = 5.6$ MeV.

S.No	N_c	T_c/MeV at $\mu = 0$	μ_c/MeV at $T = 0$	(μ_c^E, T_c^E)/MeV
01	3	235	380	(330, 81)
02	4	377	450	(415,185)
03	5	503	510	(509,271)
04	6	623	609	(604,350)

Table 3. Data for the variation in T_c and (μ_c^E, T_c^E) in the phase diagrams with various $N_f = 2$, for fixed $N_c = 3$ and $m = 5.6$ MeV.

S.No	N_f	T_c/MeV at $\mu = 0$	μ_c/MeV at $T = 0$	CEP(μ_c^E, T_c^E)/MeV
01	2	235	380	(330, 81)
02	3	216	355	(320, 64)
03	4	194	330	(308, 40)
04	5	169	300	(280, 25)

(i.e., $N_f = 2,3,4,5$). We use the same technique and same parameters to create the phase diagrams, but now we fix $N_c = 3$ and vary N_f. All the phase diagrams in Fig. 9 indicate their regular behaviors but are suppressed with increasing N_f. We note that as N_f varies, T_c, the μ_c potential, and the coordinates of the critical endpoints (μ_c^E, T_c^E) are suppressed with the increase in N_f. In Table 3, we tabulate the variation in T_c, μ_c, and (μ_c^E, T_c^E) with a large N_f.

In the next section, we summarize our findings and draw the conclusions.

VII. SUMMARY AND CONCLUSIONS

In this work, we have studied the dynamical chiral symmetry breaking/restoration for light quark flavors N_f and colors N_c. Additionally, we investigate the impact of N_c and N_f on the QCD phase diagram at finite temperature T and quark chemical potential μ. For this purpose, we use the NJL-type model dressed with the color-flavor dependence of effective coupling $\mathcal{G}^{N_c}(N_f)$ in the Schwinger-Dyson equations framework, which has advantages to study the QCD gap equation for $N_f = 0$ as well as a higher number of flavors N_f. Our observations show that for fixed $N_c = 3$ and increasing N_f, the dynamical chiral symmetry is partially restored when N_f exceeds a critical value $N_f^c \approx 8$. Our results have a remarkable resemblance with the modern lattice QCD simulation and Schwinger-Dyson's equation predictions. For $N_f = 2$, as N_c increases, we determine the critical number of colors as $N_c^c \approx 2.2$, above which the dynamical chiral symmetry is broken. The dramatic opposed effects between the two parameters N_f^c and N_c^c have been observed. This corresponds with our expectation and conforms to previous studies [22], that is, increasing N_f suppresses the dynamical generated quark mass and quark-antiquark condensate, whereas increasing N_c enhances the dynamical mass and condensate. At finite T, our results show that the dynamical chiral symmetry is restored when T reaches a critical value T_c. A higher T suppresses the dynamical quark mass and condensate in contrast to a higher N_c; consequently, the larger N_c is required for chiral symmetry breaking. Thus, the critical value N_c^c (for $N_f = 2$) increases as T increases. Our results at finite T, for fixed $N_c = 3$ and varying N_f shows that the dynamical quark mass and condensate monotonically decreases as N_f increases; hence, fewer N_f^c are required to restore the dynamical chiral symmetry at finite T. As a result, N_f^c de-

creases as T increases. The nature of the phase transition remains a crossover throughout for both phase diagrams drawn in the $N_c - T_c$ and $N_f - T_c$ planes. Similarly, in the presence of quark chemical potential μ, we conclude that the N_c^c for the dynamical chiral symmetry restoration is enhanced as μ increases and vice versa. The nature of the phase transition in this case is observed to be smooth crossover until the critical endpoint ($N_c^{cp} \approx 2.5$, $\mu_c^{cp} \approx 290$ MeV), and above that, the transition changes to the first-order. We further observe that the N_f^c required for the dynamical symmetry restoration is suppressed as μ increases. In this case, the nature of the phase transition is smooth crossover until the critical endpoint ($N_f^{cp} \approx 5, \mu_f^{cp} \approx 290$ MeV) and above that, the transition changes to the first-order.

Finally, we have sketched the QCD phase diagram in the $T-\mu$ plane for various N_c and N_f. We observe that T_c, μ_c, and the location of critical endpoint (μ_c^E, T_c^E) shift toward higher values with increasing N_c. For increasing N_f, the scenario is reversed, i.e., T_c, μ_c, and (μ_c^E, T_c^E) shift towards their lower values with the increasing N_f. We conclude that considering the number of light quark flavors (or colors) yields an important impact on the QCD phase diagram in addition to the heat bath and background fields. This work not only connects the color-flavor dependence with T and μ in congruence with the existing theoretical and phenomenological interpretations, but also has important consequences related to the heavy-ion collision experiments. In the future, we plan to investigate the color-flavor phase diagram in the presence of background fields and other light hadrons properties.

ACKNOWLEDGMENTS

We thank A. Bashir and A. Raya for their valuable suggestions and guidance during the completion of this manuscript. We acknowledge the organizers and participants of the "19th International Conference on Hadron Spectroscopy and Structure in memoriam Simon Eidelman (HADRON-2021), Mexico (online)" and "International Union of on Pure and Applied Physics (IUPAP-2022) Pakistan (online)", for providing a conducive environment for the exchange of ideas during the presentation of this work, which led to the genesis of this manuscript. We also thank the colleagues of Institute of Physics, Gomal University, for their encouragement.

APPENDIX A: FIERZ TRANSFORMATION

Fierz Transformation is a re-arrangement of fermion operator products in the Dirac, flavor, and color space using index-exchanging properties of the gamma and $SU(N_c)$ generator matrices. Consider an NJL-type interaction (for detail, see Appendix A in [41]):

$$\mathcal{L}_{\rm int} = g_I(\bar{q}\hat{\Gamma}^I q)^2 = g_I \Gamma^I_{ij}\Gamma^I_{kl}\bar{q}_i q_j \bar{q}_k q_l, \tag{A1}$$

where the operator $\hat{\Gamma}^I$ corresponds to the quark-antiquark channel I. Considering the anticommutation relation for fermions, we have the following identities

$$\begin{aligned}\mathcal{L}_{\rm exc} &= -g_I \Gamma^I_{ij}\Gamma^I_{kl}\bar{q}_i q_l \bar{q}_k q_j \ \text{ and}\\ \mathcal{L}_{qq} &= g_I \Gamma^I_{ij}\Gamma^I_{kl}\bar{q}_i \bar{q}_k q_l q_j.\end{aligned} \tag{A2}$$

In the Hartree-type approximation, we can rewrite the operators

$$\Gamma^I_{ij}\Gamma^I_{kl} = \sum_M c^I_M \Gamma^I_{ij}\Gamma^I_{kl}, \tag{A3}$$

to obtain

$$\mathcal{L}_{\rm exc} = -g_I \sum_M c^I_M (\bar{q}\hat{\Gamma}^I q)^2. \tag{A4}$$

To describe the combined effect of direct plus exchange interaction by Lagrangian, we can perform a Fierz transformation in the quark-antiquark channel:

$$\mathcal{L}_{q\bar{q}} = \mathcal{L}_{\rm dir}(\equiv \mathcal{L}_{\rm int}) + \mathcal{L}_{\rm exc} = \sum_M G_M (\bar{q}\hat{\Gamma}^I q)^2, \tag{A5}$$

where G_M represents the effective coupling constants and sum runs over all quark-antiquark channels M. G_M can be obtained from the g_I i.e, $G_M = c^I_M g_I$ for $M \neq I$ and $G_M = (1 - c^I_I) g_I$.

In the same manner, we can employ a Fierz transformation into the quark-quark channel to write the an effective quark-quark interaction as

$$\mathcal{L}_{qq} = \sum_D H_D (\bar{q}\hat{\Gamma}^D C\bar{q}^T)(q^T C\hat{\Gamma}^D q), \tag{A6}$$

where D corresponds to the various diquark channels. $H_D = d^I_D g_I$ are the quark-quark effective coupling constants. The coefficients c^I_M and d^I_D of the operators are discussed in detail in Appendix A.2 of [41]. Thus, if we know the Lagrangian $\mathcal{L}_{\rm int}$, G_M and H_D are uniquely fixed. To avoid double counting, $\mathcal{L}_{\bar{q}q}$ and $\mathcal{L}_{qq}$ are to be used in Hartree approximation only.

A simple Fierz transformation of the color-current–color-current interaction (which can be obtained from the QCD Lagrangian by converting the original $SU(N_c)$ gauge symmetry into a global symmetry of the quark color-currents) is given by

$$\mathcal{L}_{\rm int} = -g(\bar{q}\gamma^\mu \lambda^\alpha q)^2. \tag{A7}$$

The quark-antiquark interaction can be expressed as

$$\begin{aligned}\mathcal{L}_{\bar{q}q} =& \frac{2(N_c^2-1)g}{N_f N_c^2}\Big[(\bar{q}q)^2+(\bar{q}\mathrm{i}\gamma_5 q)^2-\frac{1}{2}(\bar{q}\gamma^\mu q)^2-\frac{1}{2}(\bar{q}\gamma^\mu\gamma_5 q)^2\Big]\\ &+\frac{(N_c^2-1)g}{N_c^2}\Big[(\bar{q}\tau_a q)^2+(\bar{q}\mathrm{i}\gamma_5\tau_a q)^2-\frac{1}{2}(\bar{q}\gamma^\mu\tau_a q)^2\\ &-\frac{1}{2}(\bar{q}\gamma^\mu\gamma_5\tau_a q)^2\Big]-+\frac{g}{N_c N_f}\Big[(\bar{q}\lambda_a q)^2+(\bar{q}\mathrm{i}\gamma_5\lambda_a q)^2\\ &-\frac{1}{2}(\bar{q}\gamma^\mu\lambda_a q)^2-\frac{1}{2}(\bar{q}\gamma^\mu\gamma_5\lambda_a q)^2\Big]-\frac{g}{2N_c}\Big[(\bar{q}\tau_a\lambda_{a'}q)^2\\ &+(\bar{q}\tau_a\mathrm{i}\gamma_5\lambda_{a'}q)^2-\frac{1}{2}(\bar{q}\gamma^\mu\tau_a\lambda_{a'}q)^2-\frac{1}{2}(\bar{q}\gamma^\mu\gamma_5\tau_a\lambda_{a'}q)^2\Big]\\ =&\frac{(N_c^2-1)g}{N_c^2}\sum_{a=0}^{N_f^2-1}\Big[(\bar{q}\tau_a q)^2+(\bar{q}\mathrm{i}\gamma_5\tau_a q)^2-\frac{1}{2}(\bar{q}\gamma^\mu\tau_a q)^2\\ &-\frac{1}{2}(\bar{q}\gamma^\mu\gamma_5\tau_a q)^2\Big]-\frac{g}{2N_c}\sum_{a=0}^{N_f^2-1}\Big[(\bar{q}\tau_a\lambda_{a'}q)^2+(\bar{q}\tau_a\mathrm{i}\gamma_5\lambda_{a'}q)^2\\ &-\frac{1}{2}(\bar{q}\gamma^\mu\tau_a\lambda_{a'}q)^2-\frac{1}{2}(\bar{q}\gamma^\mu\gamma_5\tau_a\lambda_{a'}q)^2\Big],\end{aligned} \tag{A8}$$

where τ_a denotes operators in the $SU(N_f)$ flavor space, and λ_a are the operators in the $SU(N_c)$ color space. The flavor and color indices run from 1 to $N_{f,c}^2-1$. Comparing the coefficient of the scalar $(\bar{q}q))^2$ and pseudo-scalar $(\bar{q}\mathrm{i}\gamma_5\tau_a q)^2$ terms from Eqs. (1) and (31), we obtain

$$G := \text{coeff.}\,(\bar{q}q)^2 = \frac{2(N_c^2-1)g}{N_f N_c^2}. \tag{A9}$$

$$G := \text{coeff.}\,(\bar{q}\mathrm{i}\gamma_5\tau_a q)^2 = \frac{(N_c^2-1)g}{N_c^2}. \tag{A10}$$

For $N_c=3$ and $N_f=2$, we obtain $G=\frac{8}{9}g$.

Now, for the quark-quark interaction, we obtain

$$\begin{aligned}\mathcal{L}_{qq} =& \frac{(N_c^2+1)g}{2N_c}[(\bar{q}\mathrm{i}\gamma_5 C\tau_A\lambda_{A'}\bar{q}^T)(q^T C\mathrm{i}\gamma_5 C\tau_A\lambda_{A'}q)\\ &+(\bar{q}C\tau_A\lambda_{A'}\bar{q}^T)(q^T C\tau_A\lambda_{A'}q)\\ &-\frac{1}{2}(\bar{q}\gamma^\mu\gamma_5 C\tau_A\lambda_{A'}\bar{q}^T)(q^T C\gamma_\mu\gamma_5 C\tau_A\lambda_{A'}q)\\ &-\frac{1}{2}(\bar{q}\gamma^\mu C\tau_A\lambda_{A'}\bar{q}^T)(q^T\gamma_\mu C\tau_A\lambda_{A'}q)]\\ &-\frac{(N_c^2-1)g}{2N_c}[(\bar{q}\mathrm{i}\gamma_5 C\tau_S\lambda_{S'}\bar{q}^T)(q^T C\mathrm{i}\gamma_5 C\tau_S\lambda_{S'}q)\\ &+(\bar{q}C\tau_S\lambda_{S'}\bar{q}^T)(q^T C\tau_S\lambda_{S'}q)\\ &-\frac{1}{2}(\bar{q}\gamma^\mu\gamma_5 C\tau_S\lambda_{S'}\bar{q}^T)(q^T C\gamma_\mu\gamma_5 C\tau_S\lambda_{S'}q)\\ &-\frac{1}{2}(\bar{q}\gamma^\mu C\tau_S\lambda_{S'}\bar{q}^T)(q^T\gamma_\mu C\tau_S\lambda_{S'}q)].\end{aligned} \tag{A11}$$

where the subscripts S and A are the symmetric and antisymmetric indices, and C is a charge conjugation operator. In particular, we obtain

$$H := \text{coeff}\,(\bar{q}\mathrm{i}\gamma_5 C\tau_A\lambda_{A'}\bar{q}^T)(q^T C\mathrm{i}\gamma_5 C\tau_A\lambda_{A'}q) = \frac{(N_c+1)g}{2N_c}. \tag{A12}$$

For $N_c=3$, we obtain $H=\frac{2}{3}g$; thus, the ratio $H:G=\frac{(N_c)}{2(N_c-1)}=\frac{3}{4}$.

References

[1] D. J. Gross and F. Wilczek, Phys. Rev. Lett. **30**, 1343-1346 (1973)
[2] H. D. Politzer, Phys. Rev. Lett. **30**, 1346-1349 (1973)
[3] K. G. Wilson, Phys. Rev. D **10**, 2445-2459 (1974)
[4] T. Appelquist, G. T. Fleming, and E. T. Neil, Phys. Rev. D **79**, 076010 (2009), arXiv:0901.3766
[5] A. Bashir, A. Raya, and J. Rodriguez-Quintero, Phys. Rev. D **88**, 054003 (2013)
[6] T. Appelquist *et al.* (LSD), Phys. Rev. D **90**, 114502 (2014), arXiv:1405.4752
[7] W. E. Caswell, Phys. Rev. Lett. **33**, 244 (1974)
[8] T. Banks and A. Zaks, Nucl. Phys. B **196**, 189-204 (1982)
[9] H. Gies and J. Jaeckel, The European Physical Journal C-Particles and Fields **46**, 433-438 (2006)
[10] T. Appelquist, G. T. Fleming, and E. T. Neil, Phys. Rev. Lett. **100**, 171607 (2008), arXiv:0712.0609
[11] A. Hasenfratz, Phys. Rev. D **82**, 014506 (2010)
[12] Y. Aoki, T. Aoyama, M. Kurachi *et al.* 2012 arXiv: 1202.4712
[13] T. Appelquist *et al.* (LSD), Phys. Rev. Lett. **104**, 071601 (2010), arXiv:0910.2224
[14] M. Hayakawa, K. I. Ishikawa, Y. Osaki *et al.*, Phys. Rev. D **83**, 074509 (2011), arXiv:1011.2577
[15] A. Cheng, A. Hasenfratz, G. Petropoulos *et al.*, JHEP **07**, 061 (2013), arXiv:1301.1355
[16] A. Hasenfratz and D. Schaich, JHEP **02**, 132 (2018), arXiv:1610.10004
[17] T. Appelquist *et al.* (Lattice Strong Dynamics), Phys. Rev. D **99**, 014509 (2019), arXiv:1807.08411
[18] T. Appelquist, A. G. Cohen, and M. Schmaltz, Phys. Rev. D **60**, 045003 (1999), arXiv:hep-th/9901109
[19] M. Hopfer, C. S. Fischer, and R. Alkofer, JHEP **11**, 035 (2014), arXiv:1405.7031
[20] A. Doff and A. A. Natale, Phys. Rev. D **94**, 076005 (2016), arXiv:1610.02564
[21] D. Binosi, C. D. Roberts, and J. Rodriguez-Quintero, Phys.

Rev. D **95**, 114009 (2017), arXiv:1611.03523
[22] A. Ahmad, A. Bashir, M. A. Bedolla *et al*., J. Phys. G **48**, 075002 (2021), arXiv:2008.03847
[23] C. Bernard, T. Burch, E. B. Gregory *et al*. (MILC), Phys. Rev. D **71**, 034504 (2005), arXiv:hep-lat/0405029
[24] M. Cheng *et al*., Phys. Rev. D **74**, 054507 (2006), arXiv:hep-lat/0608013
[25] A. Bazavov *et al*., Phys. Rev. D **85**, 054503 (2012), arXiv:1111.1710
[26] T. Bhattacharya *et al*., Phys. Rev. Lett. **113**, 082001 (2014), arXiv:1402.5175
[27] P. de Forcrand, J. Langelage, O. Philipsen *et al*., Phys. Rev. Lett. **113**, 152002 (2014), arXiv:1406.4397
[28] A. Bazavov, H. T. Ding, P. Hegde *et al*., Phys. Rev. D **95**, 074505 (2017), arXiv:1701.03548
[29] J. N. Guenther, Eur. Phys. J. A **57**, 136 (2021), arXiv:2010.15503
[30] S. x. Qin, L. Chang, H. Chen *et al*., Phys. Rev. Lett. **106**, 172301 (2011), arXiv:1011.2876
[31] C. S. Fischer, J. Luecker, and J. A. Mueller, Phys. Lett. B **702**, 438-441 (2011), arXiv:1104.1564
[32] A. Ayala, A. Bashir, C. A. Dominguez *et al*., Phys. Rev. D **84**, 056004 (2011), arXiv:1106.5155
[33] E. Gutiérrez, A. Ahmad, A. Ayala *et al*., Journal of Physics G: Nuclear and Particle Physics **41**, 075002 (2014)
[34] G. Eichmann, C. S. Fischer, and C. A. Welzbacher, Phys. Rev. D **93**, 034013 (2016), arXiv:1509.02082
[35] F. Gao and Y. x. Liu, Phys. Rev. D **94**, 076009 (2016), arXiv:1607.01675
[36] A. Ahmad and A. Raya, Journal of Physics G: Nuclear and Particle Physics **43**, 065002 (2016)
[37] C. S. Fischer, Prog. Part. Nucl. Phys. **105**, 1-60 (2019), arXiv:1810.12938
[38] C. Shi, X. T. He, W. B. Jia *et al*., JHEP **06**, 122 (2020), arXiv:2004.09918
[39] A. Ahmad, Chin. Phys. C **45**, 073109 (2021), arXiv:2009.09482
[40] S. Klevansky, Reviews of Modern Physics **64**, 649 (1992)
[41] M. Buballa, Physics Reports **407**, 205-376 (2005)
[42] P. Costa, M. C. Ruivo, C. A. De Sousa *et al*., Symmetry **2**, 1338-1374 (2010)
[43] F. Marquez, A. Ahmad, M. Buballa *et al*., Phys. Lett. B **747**, 529-535 (2015)
[44] A. Ahmad, A. Ayala, A. Bashir *et al*., J. Phys. Conf. Ser. **651**, 012018 (2015)
[45] A. Ayala, J. A. Flores, L. A. Hernandez *et al*., EPJ Web Conf. **172**, 02003 (2018), arXiv:1712.00187
[46] A. Ayala, L. A. Hernández, M. Loewe *et al*., Eur. Phys. J. A **57**, 234 (2021), arXiv:2104.05854
[47] Y. Nambu and G. Jona-Lasinio, Phys. Rev. **124**, 246 (1961)
[48] J. M. Cornwall, Phys. Rev. D **26**, 1453 (1982)
[49] A. C. Aguilar, D. Binosi, and J. Papavassiliou, Front. Phys. (Beijing) **11**, 111203 (2016), arXiv:1511.08361
[50] K. Langfeld, C. Kettner, and H. Reinhardt, Nucl. Phys. A **608**, 331-355 (1996), arXiv:hep-ph/9603264
[51] H. Kohyama 2016 arXiv: 1602.09056
[52] E. L. Solis, C. S. R. Costa, V. V. Luiz *et al*., Few Body Syst. **60**, 49 (2019), arXiv:1905.08710
[53] A. Ahmad, A. Martínez, and A. Raya, Phys. Rev. D **98**, 054027 (2018), arXiv:1809.05545
[54] A. R. Zhitnitsky, Nucl. Phys. A **813**, 279-292 (2008), arXiv:0808.1447
[55] A. R. Zhitnitsky, Nucl. Phys. A **921**, 1-18 (2014), arXiv:1308.0020
[56] O. Philipsen and J. Scheunert, JHEP **11**, 022 (2019), arXiv:1908.03136
[57] O. Philipsen and J. Scheunert, 2020 QCD in the heavy dense regime: Large N_c and quarkyonic matter *Criticality in QCD and the Hadron Resonance Gas* (*Preprint* 2011.00504)
[58] T. DeGrand, Phys. Rev. D **103**, 094513 (2021), arXiv:2102.01150
[59] B. Lucini, M. Teper, and U. Wenger, JHEP **01**, 061 (2004), arXiv:hep-lat/0307017
[60] L. McLerran and R. D. Pisarski, Nucl. Phys. A **796**, 83-100 (2007), arXiv:0706.2191
[61] R. A. Soltz, C. DeTar, F. Karsch *et al*., Ann. Rev. Nucl. Part. Sci. **65**, 379-402 (2015), arXiv:1502.02296